

Wide-band pulse-echo imaging with distributed apertures in multi-path environments

T Varslot¹, B Yazıcı¹ and M Cheney²

¹ Department of Electrical, Computer and Systems Engineering, Rensselaer Polytechnic Institute, Troy, NY, USA

² Department of Mathematical Sciences, Rensselaer Polytechnic Institute, Troy, NY, USA

E-mail: trond.varslot@anu.edu.au, yazici@ecse.rpi.edu and cheney@rpi.edu

Received 6 January 2008, in final form 29 April 2008

Published 30 June 2008

Online at stacks.iop.org/IP/24/045013

Abstract

We derive a new image reconstruction method for distributed apertures operating in complex environments. The aperture elements can be distributed spatially in an arbitrary fashion, can be several hundred wavelengths apart, and can involve transmission from multiple elements simultaneously. Moreover, the object to be imaged can be either in the near-field or far-field of the array. Our method is capable of exploiting information about multi-path scattering in the environment, statistics of the objects to be imaged and statistics of the additive (possibly non-stationary) noise. We formulate the image reconstruction problem as an inversion of a bilinear mapping that maps object reflectivity to an operator which in turn acts on the transmitted waveforms. We use transmitted waveforms to reveal the action of this bilinear mapping. We develop a minimum-norm inversion which takes the form of a family of linear operators applied to the pulse-echo measurements. This processing is implemented by means of inner products between the measurements and pre-computed quantities, separately for each receiving element. Our approach is therefore well suited for parallel implementation, and can be performed in a distributed manner.

1. Introduction

Pulse-echo imaging is generally performed by transmitting a waveform, and recording the resulting scattering from the object to be imaged. The scattering measurements are then used to form an image, which is a spatially resolved map of the object's scattering strength [1]. Pulse-echo imaging covers a wide range of applications including sonar and ultrasound, microwave, seismic and radar imaging [2–9].

High-resolution imaging techniques such as acoustic tomography or synthetic-aperture radar use a large effective aperture [5, 9]. The spatial diversity offered by these large arrays

allow a high-resolution reconstruction of extended objects. Sparse arrays, on the other hand, have mostly been used in applications where it is important to determine the location, but not the scattering characteristics, of a particular object [10, 11]. In applications of sparse arrays, the objects to be imaged are frequently regarded as point scatterers [12, 13]. However, extended objects can also be imaged by sparse arrays if the waveforms they transmit are wide band [7, 8].

In this paper, we present a new image reconstruction method that applies to pulse-echo measurements from a sparse array of transmitting and receiving elements. The array elements can be distributed spatially in an arbitrary fashion, and can be several hundred wavelengths apart. Such an array is referred to as a *distributed aperture* [14].

Distributed apertures typically view regions of interest that are not in the far-field of the array. This introduces range dependence in the scattering measurements which cannot be ignored [15, 16]. By using a physics-based measurement model we directly account not only for this range dependence but also for effects such as multi-path scattering and interference. In addition, our approach can incorporate *a priori* statistical information about the scatterers and additive noise.

We formulate the imaging problem in terms of a bilinear mapping which we refer to as the *channel mapping*. This is a mapping from the space of scattering objects to the corresponding linear operator between transmit waveforms and measured scattering. Under the *distorted wave Born approximation* (DWBA), this channel mapping is linear. We derive an inversion technique which is optimal in the sense that it minimizes the mean-square error in the reconstructed image. In doing so we allow for multiple transmitters and receivers to be activated simultaneously [17–20]. We make no additional assumptions about being able to separate the waveforms from each transmitter by orthogonality [7, 17].

We perform our image reconstruction using an appropriate set of basis functions which is adapted not only to the physical layout of our array elements, but also to the environment. Using a finite subset of these basis functions, we reconstruct a projection of the image onto a subspace spanned by this basis. The resulting numerical implementation requires only a set of inner products between the measurements and pre-computed quantities for each receiving array element. Our reconstruction algorithm, therefore, lends itself to distributed processing.

Our work is related to that of Devaney *et al*, who presented a similar reconstruction method under the assumption that the impulse response from all pairs of transmitters and receivers could be obtained for a (finite) number of frequency components [21, 22]. Our work is distinguished from these earlier papers by the fact that we formulate the problem directly in terms of time-domain pulse-echo measurements. By conducting our analysis in the time domain, we are furthermore able to account for transmit waveform diversity.

Our work is also related to that of Yazıcı *et al* [23], which used a similar general approach. However, by employing affine Fourier transforms to perform the actual inversion, that work inherently relies on the free-space propagation model, and deals with one transmitter and one receiver which are assumed to be co-located. There are no such assumptions in our current work. In fact, the ability to exploit multi-path propagation is one of the features of our work. Thus, our work generalizes the inversion technique presented in [23] to distributed apertures in a multi-path environment.

Our paper is organized as follows: in section 2, we introduce our data model, and formulate the reconstruction problem. We proceed to analyze the imaging problem under deterministic conditions in section 3. The main result for this section is theorem 1. Reconstruction in the presence of additive noise is addressed in section 4, where we incorporate second-order statistics into a minimum-norm optimal reconstruction. This is formulated in theorem 2. In section 5, we present some numerical simulations to illustrate the theoretical results and

Table 1. Definition of variables, operators, functions and function spaces.

Notation	Explanation
T_0	Positive constant which determines the maximum length of a transmit signal
V	Reflectivity function
$S(0, T_0)$	Space of transmit waveforms
$S(0, T_0)^m$	Space of transmit vectors
$s(t)$	Transmit vector, each component of which is an element of $S(0, T_0)$
$L^2(\mathbb{R})^n$	Space of measurement vectors
$m(t)$	Measurement vector, each component of which is an element of $L^2(\mathbb{R})$
\mathcal{H}	Channel mapping: operator from $L^2(\Omega)$ to linear operators between $S(0, T_0)^m$ and $L^2(\mathbb{R})^n$
$\mathcal{H}(V)$	Scattering operator or channel: operator from $S(0, T_0)^m$ to $L^2(\mathbb{R})^n$
$\text{Tr}\{A\}$	Trace of the operator A
Ω	Compact subset of \mathbb{R}^3 where all reflectivity functions have support

the performance of our image reconstruction method. Discussion and concluding remarks are found in section 6. The paper includes three appendices. Appendix A contains a brief derivation of our waveform propagation model. Appendices B and C contain proofs of some intermediate results needed for the reconstruction result in the deterministic setting, while appendix D contains the derivation of the reconstruction method in the presence of additive noise.

2. The forward model

2.1. Notational conventions

Throughout this paper we use the following font conventions: bold-face italic font (\boldsymbol{x}) denotes vector quantities, Latin capital letters in calligraphic font (\mathcal{H}) are used for operators and Latin capital letters in roman font (S) are used to denote function spaces. We use subscript index (M_{ij}, x_i) to indicate a matrix or a vector element, while we reserve superscript indices (s^k) for indexing a set of vectors. Our notation for specific variables, operators, functions and function spaces is shown in table 1.

2.2. Distributed apertures

We consider an array consisting of m transmitting elements and n receiving elements. The array elements are arbitrarily distributed, and can be several hundred wavelengths apart. These spatially distributed array elements constitute our aperture. Furthermore, we assume that we have a common reference clock for all elements. This common reference clock allows *coherent* data processing. An illustration of the distributed nature of an array with two transmitting elements and three receiving elements is shown in figure 1.

2.3. The channel model

Strictly speaking, any object with properties which deviate from a constant (homogeneous) background will produce scattering. However, scattering from an object with known location and scattering strength does not contribute new information. We therefore use the known objects to define a *background* medium. Scattering is defined in terms of deviations from this background. Our ability to observe the additional objects depends on how much the relevant

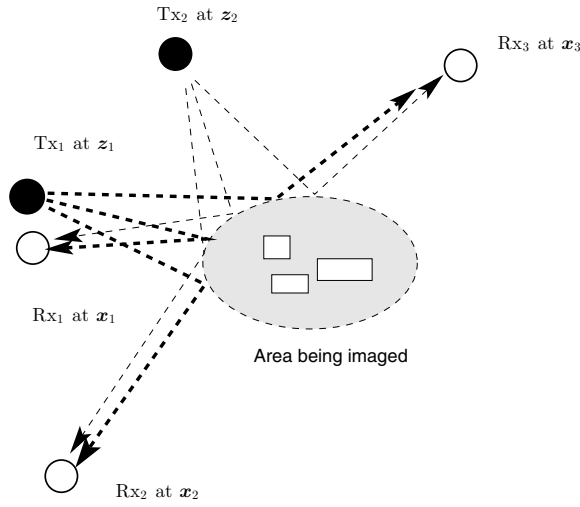


Figure 1. Distributed aperture with two transmitting elements (black circles) and three receiving elements (white circles). The transmitting elements Tx_1 and Tx_2 are located at spatial positions z_1 and z_2 , respectively. The receiving elements Rx_1 , Rx_2 and Rx_3 are located at positions x_1 , x_2 and x_3 . Arrows indicate that scattering as a result of a waveform transmitted from element Tx_1 will be measured on all receiving elements; similarly for Tx_2 .

physical properties deviate from the background. We denote this deviation by the reflectivity function $V(\mathbf{x})$. For our current work, we will assume that the propagating wave field u is described by the following scalar wave equation:

$$\nabla^2 u - \frac{1}{c^2} \partial_t^2 u = V \partial_t^2 u. \quad (1)$$

Here c is the propagation speed in the background medium. Our model for the scattering is given in terms of the *Green's function* $g(\mathbf{x}, \mathbf{y}, t)$ for the background medium. The Green's function is the response measured at position \mathbf{x} due to an impulse $\delta(t)$ transmitted from position \mathbf{y} , i.e., a solution of

$$\nabla_{\mathbf{x}}^2 g - \frac{1}{c^2} \partial_t^2 g = \delta(t) \delta(|\mathbf{x} - \mathbf{y}|). \quad (2)$$

We denote by z^j the position of the j th transmit element, and by x^i the position of the i th receive element (see figure 1). We denote by $s_j(t)$ the waveform which emanates from the j th element. We arrange the transmit waveforms in a *transmit vector* $\mathbf{s}(t)$

$$\mathbf{s}(t) := [s_1(t), \dots, s_m(t)]^T. \quad (3)$$

For a given reflectivity function V , our model for the scattering measurement $m_i(t)$ associated with the transmit vector $\mathbf{s}(t)$ is

$$m_i(t) = \sum_{j=1}^m \int g(x^i, \mathbf{y}, \tau') \partial_t^2 g(\mathbf{y}, z^j, t - \tau - \tau') V(\mathbf{y}) d\tau' d\mathbf{y} s_j(\tau) d\tau. \quad (4)$$

This model assumes that multiple reflections involving the reflectivity V may be neglected, but allows for multiple reflections in the known background medium. Equation (4) is obtained as a linearization of the Lippmann–Schwinger equation. Further details, as well as appropriate references, are found in appendix A.

We note that (4) models simultaneous transmission of different waveforms from different elements. For ease of exposition, we have assumed that each array element behaves like an isotropic point source/receiver, i.e., radiation patterns from each element do not exhibit directivity. Note that by re-interpreting the Green's function as the actual field radiated by each array element, more general antenna models may be treated within the same Green's function notation [21].

We collect the measurements into a *measurement vector* $\mathbf{m}(t)$

$$\mathbf{m}(t) := [m_1(t), \dots, m_n(t)]^T. \quad (5)$$

We refer to the mapping from transmit vector $s(t)$ to measurement vector $\mathbf{m}(t)$ as the *scattering operator* or channel, and denote it by $\mathcal{H}(V)$. By defining an $m \times n$ matrix $G(\mathbf{y}, t)$ with matrix elements

$$G_{ij}(\mathbf{y}, t) := \int g(\mathbf{x}^i, \mathbf{y}, \tau') \partial_t^2 g(\mathbf{y}, \mathbf{z}^j, t - \tau') d\tau', \quad (6)$$

we obtain a compact notation for $\mathcal{H}(V)$ as follows:

$$\mathbf{m}(t) := \mathcal{H}(V)s(t) = \int G(\mathbf{y}, t - \tau)V(\mathbf{y}) d\mathbf{y}s(\tau) d\tau. \quad (7)$$

Integration in (7) is understood to be elementwise, i.e.,

$$m_i(t) = \sum_{j=1}^m \int G_{ij}(\mathbf{y}, t - \tau)V(\mathbf{y}) d\mathbf{y} s_j(\tau) d\tau. \quad (8)$$

2.4. Problem statement and inversion strategy

The scattering operator $\mathcal{H}(V)$ is a linear mapping from transmit vectors to measurement vectors. We can now define the *channel mapping* \mathcal{H} as the linear mapping which takes the reflectivity function V to the scattering operator $\mathcal{H}(V)$. The kernel of \mathcal{H} is in this case G from (6). Furthermore, if we interchange the order of integration in (7), the inner integral defines an operator which we denote by \mathcal{G}_y :

$$\mathcal{G}_y s(t) = \int G(\mathbf{y}, t - \tau)s(\tau) d\tau, \quad (9)$$

The operator \mathcal{G}_y is the scattering operator for the reflectivity function consisting of a single delta function located at the point \mathbf{y} . With this notation, we can write

$$\mathcal{H}(V) := \int \mathcal{G}_y V(\mathbf{y}) d\mathbf{y}. \quad (10)$$

Our overall strategy is to perform imaging by inverting the mapping \mathcal{H} , i.e., we will reconstruct the reflectivity function V from knowledge of $\mathcal{H}(V)$. In order to do this, we must first construct $\mathcal{H}(V)$ from a set of transmit waveforms and corresponding measurements. For this we use a set of transmit vectors $\{s^k(t)\}$, and record the corresponding measurement vectors $\{m^k(t)\}$. From this data, we determine the action of $\mathcal{H}(V)$ on the subspace spanned by the transmit vectors $\{s^k(t)\}$.

Once the channel $\mathcal{H}(V)$ is known, we find an approximate inverse for \mathcal{H} using the Green's function for the background medium. Our image is then \tilde{V} , which, roughly speaking, is defined by

$$\tilde{V} = \mathcal{H}^{-1}\mathcal{H}(V). \quad (11)$$

2.5. Properties of the channel

In this section, we describe the assumptions and technical machinery needed for the reconstructions.

Let H_1 and H_2 be two Hilbert spaces. Furthermore, let $\{e^k\}$ be an orthonormal basis for H_1 , and denote the inner-products in H_1 and H_2 by $\langle \cdot, \cdot \rangle_1$ and $\langle \cdot, \cdot \rangle_2$, respectively. The space of Hilbert–Schmidt (HS) operators between H_1 and H_2 form a Hilbert space when equipped with the following inner product:

$$\langle \mathcal{A}, \mathcal{B} \rangle_{\text{HS}} := \sum_k \langle \mathcal{A}e^k, \mathcal{B}e^k \rangle_2. \tag{12}$$

Using $*$ to indicate the adjoint operator, we may express the inner product in terms of the trace of $\mathcal{B}^* \mathcal{A}$:

$$\langle \mathcal{A}, \mathcal{B} \rangle_{\text{HS}} = \sum_k \langle \mathcal{B}^* \mathcal{A}e^k, e^k \rangle_1 := \text{Tr}\{\mathcal{B}^* \mathcal{A}\}. \tag{13}$$

We make some appropriate assumptions on the location of the array elements, Green’s function for the medium, and transmit waveforms. These assumptions are mild enough to be valid for most applications.

Assumption 1. *Let Ω be a fixed compact subset of \mathbb{R}^3 , and let C be a fixed constant.*

- (i) *We assume that we do not measure any scattering from locations outside Ω . More precisely, we assume that the reflectivity functions are supported in Ω , and are square integrable within Ω , i.e., they are functions in $L^2(\Omega)$.*
- (ii) *We assume that all transmitter locations z^j and receiver locations x^i are outside Ω .*
- (iii) *We also assume that the background medium does not focus energy onto an arbitrarily small region; in other words, we rule out trapped rays. More precisely, let $\hat{g}(x, y, \omega)$ denote the temporal Fourier transform of the Green’s function $g(x, y, t)$. We assume that*

$$|\hat{g}(z^j, y, \omega)\hat{g}(y, x^i, \omega)| \leq C, \tag{14}$$

uniformly for all frequencies $\omega \in \mathbb{R}$, all $y \in \Omega$, and all pairs of transmitter and receiver locations (z^j, x^i) .

We note that the assumptions (ii) and (iii) can be relaxed somewhat. However, this would require additional attention to deal with the integrable singularities of the Green’s function.

Next we make some assumptions about the transmit waveforms. In order for the scattering operator to be HS, we assume that the transmit waveforms have finite energy, are of finite duration, and are approximately band limited, in the sense that their Fourier transforms decay rapidly.

Assumption 2. *Let $\rho > 0$ and $T_0 > 0$ be predetermined constants. We assume that the space $S(0, T_0)$ of transmit waveforms is a subset of the Sobolev space $\mathring{H}^{(5+\rho)/2}(0, T_0)$.*

Here $H^{(5+\rho)/2}(\mathbb{R})$ consists of functions s whose Fourier transforms $\hat{s}(\omega)$ satisfy

$$\int (1 + |\omega|^{5+\rho})|\hat{s}(\omega)|^2 d\omega < \infty \tag{15}$$

and $\mathring{H}^{(5+\rho)/2}(0, T_0)$ is the subspace of $H^{(5+\rho)/2}(\mathbb{R})$ of functions with support in $[0, T_0]$.

On the space $S(0, T_0)$, as defined in assumption 2, we will use the $H^{(5+\rho)/2}(\mathbb{R})$ inner product

$$\langle f, g \rangle_s := \int (1 + |\omega|^{5+\rho})\hat{f}(\omega)\overline{\hat{g}(\omega)} d\omega. \tag{16}$$

Assumption 3. Let S be as stated in assumption 2. Let $S_K(0, T_0)^m$ be the subspace of $S(0, T_0)^m$ which is spanned by the transmit vectors

$$\{s^1(t) \cdots s^K(t)\}, \quad (17)$$

where each of the vectors have elements which are supported on $[0, T_0]$.

Assumption 4. We assume that $\{s^k\}$ is a set of orthonormal basis functions for the transmit-vector space $S(0, T)^m$. The corresponding measurements are denoted by $\{m^k\}$.

Lemma 1. Under assumptions 1 and 2, for each reflectivity function $V \in L^2(\Omega)$ the scattering operator $\mathcal{H}(V)$ is a Hilbert–Schmidt operator from transmit vectors with elements in $S(0, T_0)$ to measurement vectors with elements in $L^2(\mathbb{R})$.

We provide a proof of lemma 1 in appendix B.

3. Imaging under deterministic conditions

In this section we derive an imaging algorithm which offers a minimum-norm reconstruction of the reflectivity function V under the assumption that there is no measurement noise. Our reconstruction method for this case is stated in theorem 1 in section 3.2.

3.1. Replacing the scattering operator by measurements

Our imaging method is derived from applying an approximate inverse of the operator \mathcal{H} to the operator $\mathcal{H}(V)$. The measurement vector obtained from transmitting a certain transmit vector tells us directly what the action of $\mathcal{H}(V)$ is on the subspace spanned by this transmit vector. If we transmit an orthonormal basis for the space of transmit vectors, we are essentially mapping out the whole operator $\mathcal{H}(V)$. However, we do not explicitly construct $\mathcal{H}(V)$. Rather, we base our inversion on the directly available scattering measurement vectors.

3.2. Imaging by inversion of the channel mapping \mathcal{H}

In this section, we develop a general method for reconstructing the reflectivity function V from knowledge of $\mathcal{H}(V)$.

Lemma 1 implies that the mapping \mathcal{H} is a linear operator from the Hilbert space of reflectivity functions, $L^2(\Omega)$, to the Hilbert space of scattering operators. The minimum-norm solution for the inversion problem is therefore provided by the pseudo-inverse \mathcal{H}^\dagger of \mathcal{H} [24]. We obtain our image of the reflectivity function as

$$\tilde{V} = \mathcal{H}^\dagger \mathcal{H}(V). \quad (18)$$

In this paper we use the pseudo-inverse $\mathcal{H}^\dagger = (\mathcal{H}^* \mathcal{H})^\dagger \mathcal{H}^*$. We therefore establish below a way to compute the adjoint of \mathcal{H} . As it turns out, we are able to express the adjoint directly in terms of the Green's function of the background medium. This result is stated in the third part of the following lemma.

Lemma 2. Under assumptions 1 and 2, the following hold:

- (i) $\mathcal{G}_y : S(0, T_0)^m \rightarrow L^2(\mathbb{R})^n$ is a bounded linear operator for each y .
- (ii) The family of bounded linear operators $\{\mathcal{G}_y\}_{y \in \Omega}$ is uniformly bounded.
- (iii) The adjoint of \mathcal{H} evaluated at \mathcal{A} is $[\mathcal{H}^* \mathcal{A}](y) = \overline{\text{Tr}\{\mathcal{G}_y \mathcal{A}^*\}}$, where the trace is defined in (13). Here \mathcal{A} denotes a Hilbert–Schmidt operator from the space $S(0, T_0)^m$ of transmit vectors to the space $L^2(\mathbb{R})^n$ of measurement vectors.

We prove lemma 2 in appendix C.

Lemma 3. *Under assumptions 1 and 2, the operator \mathcal{H}^* is bounded.*

Proof. To see that \mathcal{H}^* is bounded we apply \mathcal{H}^* to an HS operator \mathcal{A} and compute the norm of the result as follows:

$$\|\mathcal{H}^*\mathcal{A}\|_2^2 = \int |\mathcal{H}^*\mathcal{A}(x)|^2 dx = \int_{\Omega} \left| \sum_k \langle \mathcal{A}s^k, \mathcal{G}_x s^k \rangle \right|^2 dx \leq \int_{\Omega} \sum_k |\langle \mathcal{A}s^k, \mathcal{G}_x s^k \rangle|^2 dx. \quad (19)$$

To the right-hand side, we apply the Cauchy–Schwarz inequality to obtain

$$\|\mathcal{H}^*\mathcal{A}\|_2^2 \leq \int_{\Omega} \sum_k \langle \mathcal{A}s^k, \mathcal{A}s^k \rangle \langle \mathcal{G}_x s^k, \mathcal{G}_x s^k \rangle dx. \quad (20)$$

From lemma 2 we now use the result that \mathcal{G}_x is a uniformly bounded family. Let an upper bound for their norm be C_0 . Then

$$\langle \mathcal{G}_x s^k, \mathcal{G}_x s^k \rangle \leq C_0, \quad (21)$$

since the transmit vectors are assumed to be of unit norm. Thus, we rewrite (20) as

$$\|\mathcal{H}^*\mathcal{A}\|_2^2 \leq \sum_k \langle \mathcal{A}s^k, \mathcal{A}s^k \rangle C_0 \int_{\Omega} dx \quad (22)$$

$$= C_0^2 n \|\mathcal{A}\|_{\text{HS}}^2 \int_{\Omega} dx. \quad (23)$$

The last integral is finite since Ω is compact. Therefore \mathcal{H}^* is a bounded operator. This concludes the proof of lemma 3. \square

We next obtain an expression for the pseudo-inverse \mathcal{H}^\dagger needed for our inversion method given in (18). We do so in several steps: (1) first we apply \mathcal{H}^* to $\mathcal{H}(V)$ and obtain an expression for the operator $\mathcal{H}^*\mathcal{H}$. (2) Next we use eigenfunctions of $\mathcal{H}^*\mathcal{H}$ to determine a singular-value decomposition (SVD) of \mathcal{H} [24]. (3) Finally we state our inversion algorithm in terms of the SVD of \mathcal{H} .

Step 1. In order to obtain a useful expression for the pseudo-inverse \mathcal{H}^\dagger appearing in (18), we need the following fact.

Lemma 4. *Under assumptions 1–3, the operator $\mathcal{H}^*\mathcal{H}$ is bounded and self-adjoint, and has kernel $\text{Tr}\{\mathcal{G}_x^* \mathcal{G}_y\}$.*

Proof. The operator $\mathcal{H}^*\mathcal{H}$ is obviously self-adjoint. Boundedness follows from the boundedness of \mathcal{H}^* (see lemma 3). To obtain an expression for the kernel, we use (10) and (13) to obtain

$$[\mathcal{H}^*\mathcal{H}(V)](x) = \overline{\text{Tr}\{\mathcal{G}_x \mathcal{H}(V)^*\}} = \sum_k \langle \mathcal{H}(V)s^k, \mathcal{G}_x s^k \rangle. \quad (24)$$

$$= \sum_k \langle \mathcal{G}_x^* \mathcal{H}(V)s_k, s_k \rangle \quad (25)$$

$$= \int \left(\sum_k \langle \mathcal{G}_x^* \mathcal{G}_y s_k, s_k \rangle \right) V(y) dy \quad (26)$$

$$= \int \text{Tr}\{\mathcal{G}_x^* \mathcal{G}_y\} V(y) dy, \quad (27)$$

Step 2. Below we obtain an inversion of $\mathcal{H}^*\mathcal{H}$ using the measurements corresponding to the action of $\mathcal{H}(V)$ on the finite-dimensional space of transmit vectors. Note, however, that even though $\mathcal{H}(V)$ has finite-dimensional range, the operator \mathcal{H} does not; the space of HS operators between transmit vectors and measurements is infinite dimensional. What the finite-dimensionality assumption does for us is to reduce $\text{Tr}\{\mathcal{G}_x^*\mathcal{G}_y\}$ to a finite sum, terms of which, by part (iii) of assumption 1, are each square integrable. This implies that the kernel of $\mathcal{H}^*\mathcal{H}$ is square integrable, which in turn implies that $\mathcal{H}^*\mathcal{H}$ is compact.

Spectral decomposition of $\mathcal{H}^\mathcal{H}$.* Under assumptions 1–3, $\mathcal{H}^*\mathcal{H}$ has a spectral representation in terms of a discrete set of orthogonal eigenfunctions. Let $\{(\lambda_p, U_p)\}$ be the set of non-zero eigenvalues and associated orthonormal eigenfunctions for $\mathcal{H}^*\mathcal{H}$

$$\mathcal{H}^*\mathcal{H}(U_p) = \lambda_p U_p. \quad (28)$$

These eigenfunctions can be thought of as a basis of functions out of which we will construct the reflectivity function V . We will always assume that the eigenvalues are ordered according to their size, i.e., $\lambda_p \geq \lambda_{p+1}$. We define a set of operators \mathcal{U}_p by

$$\mathcal{U}_p = \frac{1}{\sqrt{\lambda_p}} \mathcal{H}(U_p), \quad (29)$$

where the action of \mathcal{U}_p on a waveform s is obtained by using (7). The operators \mathcal{U}_p are the normalized scattering operators associated with the ‘eigenscatterers’ U_p .

Step 3. With this notation, we can now state the reconstruction theorem.

Theorem 1. *Let \mathcal{H} and its adjoint \mathcal{H}^* be as defined in lemma 2.*

Under assumptions 1–4, the minimum-norm least-square-error reconstruction $\tilde{V}(\mathbf{x})$ for the reflectivity function $V(\mathbf{x})$ is given by

$$\tilde{V}(\mathbf{x}) = (\mathcal{H}^*\mathcal{H})^\dagger \mathcal{H}^*\mathcal{H}(V)(\mathbf{x}) = \sum_p \frac{1}{\sqrt{\lambda_p}} \sum_{k=1}^K \langle \mathbf{m}^k, \mathcal{U}_p \mathbf{s}^k \rangle U_p(\mathbf{x}), \quad (30)$$

where λ_p and U_p satisfy

$$\lambda_p U_p(\mathbf{x}) = \int \left(\sum_k \langle \mathcal{G}_x^* \mathcal{G}_y \mathbf{s}_k, \mathbf{s}_k \rangle \right) U_p \, d\mathbf{y}. \quad (31)$$

Here \mathcal{U}_p is given by (29) and $\mathcal{G}_x^* \mathcal{G}_y$ is defined in (28).

Proof. First we note that from (24) and the fact that $\mathcal{H}(V) \mathbf{s}^k$ is precisely the measurement \mathbf{m}^k resulting from transmitting waveform \mathbf{s}^k , we have

$$[\mathcal{H}^*\mathcal{H}(V)](\mathbf{x}) = \sum_k \langle \mathbf{m}^k, \mathcal{G}_x \mathbf{s}^k \rangle. \quad (32)$$

From the spectral decomposition of $\mathcal{H}^*\mathcal{H}$, we obtain

$$\tilde{V} = (\mathcal{H}^*\mathcal{H})^\dagger \mathcal{H}^*\mathcal{H}(V) = \sum_p \frac{1}{\lambda_p} \langle [\mathcal{H}^*\mathcal{H}(V)], U_p \rangle U_p. \quad (33)$$

From (32), (9) and (10), we compute

$$\langle [\mathcal{H}^* \mathcal{H}(V)], U_p \rangle = \left\langle \sum_k \langle \mathbf{m}^k, \mathcal{G}_y \mathbf{s}^k \rangle, U_p \right\rangle = \sum_{k=1}^K \int \langle \mathbf{m}^k, \mathcal{G}_y \mathbf{s}^k \rangle \overline{U_p(\mathbf{y})} \, d\mathbf{y} \quad (34)$$

$$= \sum_{k=1}^K \langle \mathbf{m}^k, \mathcal{H}(U_p) \mathbf{s}^k \rangle = \sum_{k=1}^K \sqrt{\lambda_p} \langle \mathbf{m}^k, \mathcal{U}_p \mathbf{s}^k \rangle. \quad (35)$$

□

Theorem 1 yields an operator which we can apply to scattering measurements $\{\mathbf{m}^k\}$ in order to reconstruct the image. However, as it stands, the operator is unbounded, because the singular values λ_p converge to zero as $p \rightarrow \infty$. Consequently, the reconstruction operator given in (30) is not expected to perform well (or even be defined) if the scattering measurements contain noise or other errors. In practical applications some form of regularization of (30) is needed in order to make the reconstruction more robust, e.g., truncate the summation over p to only include terms such that $\lambda_p > \rho$ for some $\rho > 0$. Issues pertaining to reconstruction in the presence of additive noise are discussed in section 4.

3.3. Algorithmic description of the imaging method

We have constructed a set of basis functions $\{U_p\}$ which are adapted to our distributed aperture and to the environment. Each such basis function is a unit-norm reflectivity function. The scattered field from U_p is $\sqrt{\lambda_p} \mathcal{U}_p \mathbf{s}^k$ when a transmit vector \mathbf{s}^k is employed. We therefore obtain our reconstruction by matching each measurement against fields $\mathcal{U}_p \mathbf{s}^k$, whereby we determine the component of the total scattering that is produced by the reflectivity U_p . For each transmit vector this procedure is repeated with all the basis functions. The results are combined to a single reconstruction using weights determined by the singular values $\sqrt{\lambda_p}$.

An algorithmic description of our reconstruction method is given below:

- (i) Select a set of K orthonormal transmit vectors $\{\mathbf{s}_k\} \subset S(0, T_0)^m$.
- (ii) From the Green's function for the background medium we compute

$$\text{Tr}\{\mathcal{G}_x^* \mathcal{G}_y\} \equiv \sum_{k=1}^K \langle \mathcal{G}_x^* \mathcal{G}_y \mathbf{s}_k, \mathbf{s}_k \rangle, \quad (36)$$

where $\mathcal{G}_x^* \mathcal{G}_y$ is given in (28).

- (iii) Determine the eigenvalues and eigenfunctions (λ_p, U_p) of the integral operator with kernel $\text{Tr}\{\mathcal{G}_x^* \mathcal{G}_y\}$.
- (iv) Determine the associated operators \mathcal{U}_p of \mathcal{H} according to (29).
- (v) Transmit the vectors \mathbf{s}^k and obtain the associated measurement vectors \mathbf{m}^k .
- (vi) Match each measurement \mathbf{m}^k with $\mathcal{U}_p \mathbf{s}^k$, and reconstruct according to a suitably regularized version of (30).

This algorithm depends on our ability to compute $\text{Tr}\{\mathcal{G}_x \mathcal{G}_y\}$, and hence on the nature of the Green's functions and the transmit waveforms involved. First, we note that $\mathcal{G}_x \mathbf{s}_k$ is a hypothetical scattering measurement that would be obtained when the field due to the transmit vector \mathbf{s}_k scatters from a point reflector located at position \mathbf{x} . Under assumption 1, we avoid integrating over the singularities of the Green's function when computing these hypothetical measurements. Furthermore, by assumption 2, the transmit waveforms are assumed to be smooth. Therefore, we can compute these hypothetical measurements numerically as long as basic sampling criteria are met. Furthermore, as we have limited high-frequency content in

our transmit waveforms, diffraction of the propagating wave will ensure that \mathcal{G}_x is a smooth function of x . The quantity $\text{Tr}\{\mathcal{G}_x\mathcal{G}_y\}$ is at this point a finite sum of (temporal) inner products between such measurements, and therefore well behaved as a function of x and y .

The functions $\{U_p\}$ provide an orthogonal basis for the reconstruction. Furthermore, by virtue of being eigenfunctions of $\mathcal{H}^*\mathcal{H}$, they yield a representation of the reflectivity function where the terms associated with large eigenvalues correspond to the most visible parts. In this sense, computing a reconstruction based on only the terms corresponding to the largest eigenvalues yield an image which represents a projection of the true reflectivity function onto a subspace where the aperture has the best sensitivity—sensitivity being quantified by the L^2 norm of the scattered signal that is measured. By orthogonality we furthermore know that each additional term which is computed for our imaging algorithm provides reconstruction of the reflectivity function in a new subspace of $L^2(\Omega)$. In this sense our reconstruction is efficient.

If the template fields $U_p s^k$ are computed off-line, the inversion is efficiently implemented as a set of inner-products independently computed for each array element. This means that a significant part of the computation can be performed in a decentralized fashion on each array element. Furthermore, as the reconstructed reflectivity function is expanded in terms of the basis functions, only the coefficients in this expansion need to be communicated from each element. This combination of distributed processing and compressed information representation is desirable in applications where the communication bandwidth from each aperture element is limited.

4. Imaging under uncertainty

Our inversion operator in theorem 1 yields the minimum-norm solution which attains the smallest reconstruction error when the measurements do not contain noise, i.e., when we know the scattering exactly. In this section we consider measurements which are contaminated by additive noise. We will use the second-order statistical information about the reflectivity function in order to design a reconstruction method which is optimal for noise-contaminated measurements. Optimality will be defined in terms of the *mean-square error* (MSE).

We assume that we have measurements m^k which are contaminated by noise, i.e.,

$$m^k(t) = \mathcal{H}(V)s^k(t) + n(t). \quad (37)$$

Our assumptions about the statistics of the reflectivity function and the noise are as follows.

Assumption 5. *The reflectivity function is a realization of a zero-mean random field with finite variance and continuous covariance function*

$$R_V(y_1, y_2) = E[V(y_1)\overline{V(y_2)}]. \quad (38)$$

Assumption 6. *The additive noise $n(t)$ is assumed to be a zero-mean stochastic vector process with known covariance function:*

(i) *The cross-covariance between the noise in the measurements at elements i and j is*

$$E[n_i(t_1)\overline{n_j(t_2)}] = R_i(t_1, t_2)\delta_{ij}. \quad (39)$$

(ii) *The covariance function satisfies one of the following conditions:*

(a) *non-stationary noise: $\int R_i(t, t) dt < \infty$;*

(b) *stationary noise: $R_i(t_1, t_2) = R_i(t_2 - t_1, 0)$, and $\int |R_i(t, 0)| dt < \infty$.*

(iii) *The measurement noise and the reflectivity function are statistically uncorrelated.*

Under assumption 5, we can express the reflectivity function in terms of the Karhunen–Loève (KL) expansion [25]

$$V(\mathbf{x}) = \sum_r c_r V_r(\mathbf{x}). \quad (40)$$

Here $\{V_r\}$ is a set of orthonormal L^2 -functions, and c_r are independent random variables. Furthermore, the sequence $\{E[|c_r|^2]\}$ is square summable.

We seek a linear reconstruction method that will suppress noise and that can accommodate prior statistical information about the reflectivity. Since \mathcal{H}^* is invertible on the range of \mathcal{H} , we can without loss of generality assume that our linear reconstruction method is of the form:

$$V^B = \mathcal{B}\mathcal{H}^*[\mathcal{H}(V)], \quad (41)$$

where \mathcal{B} is a suitable linear operator on $L^2(\Omega)$. We already know from (32) how to express \mathcal{H}^* applied to $\mathcal{H}(V)$ in terms of noise-free measurements \mathbf{m}_k . A natural way to approach the reconstruction for the noise-contaminated case is therefore to substitute the noisy data into (32) and then use \mathcal{B} to filter out the noise component of the reconstruction in the image domain. In order to do so we define \mathcal{B} below in terms of the statistics of the noise and the reflectivity.

In the absence of noise we want the operator \mathcal{B} to coincide with the deterministic solution from theorem 1. Therefore, we exclude the part of V that lies in the null space of \mathcal{H} when defining the MSE of the reconstruction:

$$\text{MSE}(\mathcal{B}) := \int E[|V^B(\mathbf{x}) - PV(\mathbf{x})|^2] d\mathbf{x}, \quad (42)$$

where P is the projection onto the range of \mathcal{H}^*

$$PV(\mathbf{x}) := \sum_p \langle V, U_p \rangle U_p(\mathbf{x}) = \sum_r c_r \sum_p \langle V_r, U_p \rangle U_p(\mathbf{x}), \quad (43)$$

and the sum is defined in the mean-square sense and where the U_p were defined are in (28). The second equality of (43) is obtained by inserting the KL expansion of V from (40).³ The projection PV is therefore obtained by simply projecting each $V_r(\mathbf{x})$ onto the subspace spanned by the functions $\{U_p(\mathbf{x})\}$, i.e., projecting onto the range of \mathcal{H}^* .

Our goal is to determine \mathcal{B} such that the MSE in (42) is minimized. The reconstruction formula for the statistical case is then given in the following theorem:

Theorem 2. *Let $\{s^1(t), \dots, s^K(t)\}$ be a set of orthonormal vectors in the space of transmit vectors $S(0, T_0)^m$. Let $\{\mathbf{m}^1(t), \dots, \mathbf{m}^K(t)\}$ be the corresponding measurements*

$$\mathbf{m}^k(t) = \mathcal{H}(V)s^k(t) + \mathbf{n}(t). \quad (44)$$

If the first- and second-order statistics of the additive noise and the reflectivity function satisfy assumptions 6 and 5, then the linear MMSE reconstruction \tilde{V} of the reflectivity function V is given by

$$\tilde{V} = \mathcal{M}\mathcal{S}^{\frac{1}{2}}(\mathcal{S}^{\frac{1}{2}}\mathcal{M}\mathcal{S}^{\frac{1}{2}} + \mathcal{E})^{\dagger}\mathcal{S}^{-\frac{1}{2}}\mathcal{H}^*[\mathcal{H}(V)]. \quad (45)$$

In terms of the scattering measurements $\{\mathbf{m}^k\}$ and the basis functions $\{U_p\}$ defined in (28), the adjoint \mathcal{H}^ of \mathcal{H} can be computed as in (32), and the operators \mathcal{M} , \mathcal{S} and \mathcal{E} have coefficients*

$$(\mathcal{M})_{ij} = \sum_r E[|c_r|^2] \langle V_r, U_i \rangle \overline{\langle V_r, U_j \rangle}, \quad (46)$$

³ We are justified in interchanging the order of summation since $E[|c_r|^2]$ is square summable, and $\{V_r\}$ and $\{U_p\}$ are square integrable.

$$(\mathcal{S})_{ij} = \delta_{ij}\lambda_i, \quad (47)$$

$$(\mathcal{E})_{ij} = \text{Tr}\{\mathcal{U}_i^* \mathcal{R}_n \mathcal{U}_j\}. \quad (48)$$

Here \mathcal{R}_n is an operator where the kernel is a diagonal matrix with functions $R_i(t_1, t_2)$ from (39) along the diagonal.

We prove theorem 2 in appendix D.

Inserting (45) into (D.18) from the proof of theorem 2, we obtain the following expression for the resulting MMSE:

$$\text{MSE}(\mathcal{B}) = \text{Tr}\{\mathcal{M} - \mathcal{M}\mathcal{S}^{1/2}(\mathcal{S}^{1/2}\mathcal{M}\mathcal{S}^{1/2} + \mathcal{E})^\dagger \mathcal{S}^{1/2}\mathcal{M}\}. \quad (49)$$

We observe that we obtain the result of theorem 1 from (45) when no additive noise is present.

If the additive noise is white, then \mathcal{E} is a diagonal operator. Furthermore, if the elements of our aperture are spatially distributed in such a fashion that the basis functions $\{U_p\}$ correspond to the basis functions $\{V_p\}$ in the KL expansion for our reflectivity function model, we see that $\langle U_p, V_q \rangle = \delta_{pq}$. Therefore, the optimal reconstruction in the presence of noise in this case can be obtained by Tikhonov regularization of the inversion formula given in (30), i.e.,

$$\tilde{V}(\mathbf{x}) = \sum_p \frac{\sqrt{\lambda_p}}{\lambda_p + \sigma_p^2} \sum_{k=1}^K \langle \mathbf{m}^k, \mathcal{U}_p \mathbf{s}^k \rangle U_p(\mathbf{x}). \quad (50)$$

If the reflectivity function has non-zero mean, the MMSE reconstruction formula of (45) can be obtained by using a minimum variance estimation criterion. In this case the MSE includes a bias term in addition to that given in (42) [26].

5. Analytic examples and numerical simulations

In this section we present analytic examples and numerical simulations to demonstrate the performance and properties of our reconstruction method. In section 5.1 we discuss two cases which are simple enough to be treated analytically. We then proceed to show numerical results for these two cases in section 5.2.

5.1. Analytic examples

5.1.1. Free-space background. We first consider a scenario where the background is free space. For this case the Green's function is

$$g(\mathbf{x}, \mathbf{y}, t) = \frac{\delta(t - |\mathbf{x} - \mathbf{y}|/c)}{4\pi|\mathbf{x} - \mathbf{y}|}, \quad (51)$$

where δ is the Dirac delta function. Combining (51) with (6), we see that the kernel of our channel mapping \mathcal{H} is

$$G_{ij}(\mathbf{y}, t) = \frac{\delta(t - [|\mathbf{x}^i - \mathbf{y}| + |\mathbf{y} - \mathbf{z}^j|/c])}{16\pi^2|\mathbf{x}^i - \mathbf{y}||\mathbf{y} - \mathbf{z}^j|} \partial_t^2. \quad (52)$$

Furthermore, if we use f'' to denote the second derivative of f , then the quantity \mathcal{G}_y from lemma 2 is

$$[\mathcal{G}_y f]_{ij}(t) = \frac{f''(t - [|\mathbf{x}^i - \mathbf{y}| + |\mathbf{y} - \mathbf{z}^j|/c])}{16\pi^2|\mathbf{x}^i - \mathbf{y}||\mathbf{y} - \mathbf{z}^j|}. \quad (53)$$

From this, it is clear that (32) in the free-space case becomes

$$[\mathcal{H}^*\mathcal{H}(V)](\mathbf{x}) = \sum_{k,i,j} \int \frac{(s^k)_j''(t - \Delta_{ij}(\mathbf{x}))}{16\pi^2|\mathbf{x}^i - \mathbf{x}||\mathbf{x} - \mathbf{z}^j|} (m^k)_i(t) dt \quad (54)$$

$$= \sum_{k,i,j,l} \int \frac{(s^k)_j''(t - \Delta_{ij}(\mathbf{x}))}{16\pi^2|\mathbf{x}^i - \mathbf{x}||\mathbf{x} - \mathbf{z}^j|} \frac{(s^k)_l''(t - \Delta_{il}(\mathbf{y}))}{16\pi^2|\mathbf{x}^i - \mathbf{y}||\mathbf{y} - \mathbf{z}^l|} V(\mathbf{y}) d\mathbf{y} dt. \quad (55)$$

Here $\Delta_{ij}(\mathbf{x}) = (|\mathbf{x}^i - \mathbf{x}| + |\mathbf{x} - \mathbf{z}^j|)/c$ denotes the travel time from the transmitter at location \mathbf{z}^j via the location \mathbf{y} and back to the receiver at location \mathbf{x}^i .

The integral operator $\mathcal{H}^*\mathcal{H}$ is now

$$[\mathcal{H}^*\mathcal{H}(V)](\mathbf{x}) = \int \Xi(\mathbf{x}, \mathbf{y}) V(\mathbf{y}) d\mathbf{y} \quad (56)$$

with kernel

$$\Xi(\mathbf{x}, \mathbf{y}) = \sum_{i,j,l,k} \Xi_{ijl}(\mathbf{x}, \mathbf{y}, s^k) \quad (57)$$

$$\Xi_{ijl}(\mathbf{x}, \mathbf{y}, s) = \frac{\langle s_l''(\cdot + \Delta_{ij}(\mathbf{x}) - \Delta_{il}(\mathbf{y})), s_j'' \rangle}{256\pi^4|\mathbf{x}^i - \mathbf{x}||\mathbf{x} - \mathbf{z}^j||\mathbf{x}^i - \mathbf{y}||\mathbf{y} - \mathbf{z}^l|}. \quad (58)$$

We see that the kernel is a weighted sum of appropriately delayed auto- and cross-ambiguity functions between second derivatives of the transmit waveforms. The emergence of the second derivatives in these expressions is due to our particular wave equation and scattering model (see appendix A). In the narrow-band case, this differentiation is approximately multiplication by a constant (namely, the negative of the square of the carrier frequency), leading to an approximate representation by delayed and weighted inner products between the different transmit waveforms.

Our reconstruction method is then based on determining the eigenfunctions of (56). We use the corresponding eigenvalues to design an inverse filter which recovers the reflectivity function V .

5.1.2. Simple multi-path background. A simple multi-path scenario, which can be treated analytically, is the case where we have an infinite reflecting plane, on which a Dirichlet boundary condition (i.e., the field is zero) holds. Without loss of generality we assume that the reflecting plane is described by $[x_1, x_2, 0]$, i.e., it is perpendicular to the third coordinate axis. This is shown as a solid straight line in figure 2.

For each location $\mathbf{x} = [x_1, x_2, x_3]^T$ we introduce a *mirror location* $\mathbf{x}' = [x_1, x_2, -x_3]^T$ on the other side of the reflecting plane. In figure 2 we have given the mirror locations primed labels. Using this notation, and assuming that our propagating wave satisfies Dirichlet boundary conditions at the reflecting plane, the Green's function for this scenario is

$$g(\mathbf{x}, \mathbf{y}, t) = \frac{\delta(t - |\mathbf{x} - \mathbf{y}|/c)}{4\pi|\mathbf{x} - \mathbf{y}|} - \frac{\delta(t - |\mathbf{x} - \mathbf{y}'|/c)}{4\pi|\mathbf{x} - \mathbf{y}'|}. \quad (59)$$

Thus, the field that is radiated into the scene from our idealized point antenna elements is

$$\sum_j g(\mathbf{y}, \mathbf{z}^j, t) = \sum_j \frac{s_j(t - |\mathbf{y} - \mathbf{z}^j|/c)}{4\pi|\mathbf{y} - \mathbf{z}^j|} - \frac{s_j(t - |\mathbf{y} - \mathbf{z}'^j|/c)}{4\pi|\mathbf{y} - \mathbf{z}'^j|}. \quad (60)$$

Let $z_*^j \in \{z^1, \dots, z^m, z^{*1}, \dots, z^{*m}\}$ be the location or the mirror location of a transmit element. Let furthermore $s_{*j} \in \{s_1, \dots, s_m, -s_1, \dots, -s_m\}$ be the transmit waveform from location z_*^j . It is clear that the radiated field in (60) can be expressed as

$$\sum_{j=1}^m g(\mathbf{y}, z_*^j, t) = \sum_{j=1}^{2m} \frac{s_{*j}(t - |\mathbf{y} - z_*^j|/c)}{4\pi |\mathbf{y} - z_*^j|}. \quad (61)$$

Therefore, this field can be created in a free-space environment if we add a mirror element for each physical array element, i.e., double the number of elements.

The scattering is analyzed similarly to the free-space case by adding a receiver at the mirror location of each physical receiver. We therefore define an augmented set of receiver locations $\mathbf{x}_*^i \in \{\mathbf{x}^1, \dots, \mathbf{x}^n, \tilde{\mathbf{x}}_1, \dots, \tilde{\mathbf{x}}^m\}$. In order to obtain the multi-path scattering measurement, we add the free-space scattering measurements at $\tilde{\mathbf{x}}^i$ and \mathbf{x}_i . Thus, the scattering model in (4) is

$$m_i(t) = (\mathcal{H}(V)s_k)_i = \sum_{j=1}^{2m} \int \frac{(s^k)''_{*j}(t - \Delta_{*ij}(\mathbf{x}))}{16\pi^2 |\mathbf{x}_*^i - \mathbf{x}| |\mathbf{x} - z_*^j|} + \frac{(s^k)''_{*j}(t - \Delta_{*(i+n)j}(\mathbf{x}))}{16\pi^2 |\mathbf{x}_*^{(i+n)} - \mathbf{x}| |\mathbf{x} - z_*^j|}, \quad (62)$$

where $\Delta_{*ij}(\mathbf{x})$ is defined as in (55), with \mathbf{x}_*^i and z_*^j . We see that we get four types of scattering events:

- (i) Direct path: transmitter \rightarrow reflectivity function \rightarrow receiver. These are the terms where no mirror coordinates occur in the free-space equivalent model.
- (ii) One bounce: transmitter \rightarrow wall \rightarrow reflectivity function \rightarrow receiver. These are the terms where the transmitter is at a mirror coordinate in the free-space equivalent model.
- (iii) One bounce: transmitter \rightarrow reflectivity function \rightarrow wall \rightarrow receiver. These are the terms where the receiver is at a mirror location in the free-space equivalent model.
- (iv) Two bounces: transmitter \rightarrow wall \rightarrow reflectivity function \rightarrow wall \rightarrow receiver. These are the terms where both transmitter and receiver are at a mirror location in the free-space equivalent model.

These different multi-path scattering events are discussed in [27]. Computation of $\mathcal{H}^*\mathcal{H}$ can now be performed in a straight-forward manner as in (56), but is omitted here as the insight gained from these expressions do not justify the space.

5.2. Numerical examples

In order to demonstrate the performance of our reconstruction method, we conducted a set of numerical simulations for a square object in two different scenarios. First we simulated scattering from an object in a free-space background. Then we performed another simulation where we inserted a mirror surface behind the object to be imaged (see figure 2). These two scenarios correspond to the analytic examples given in section 5.1. Linearity of the reconstruction method implies that the results can be extrapolated to more complex objects by approximating them as a linear combination of squares.

We used a distributed aperture with two transmit elements and up to 10 receive elements. The antenna elements were equally spaced on a semicircle with radius 10λ . The object which we wanted to image was a square with sides of 1.5λ . We reconstructed this reflectivity on a 50×50 grid covering a region of $5\lambda \times 5\lambda$ around the square. The true reflectivity that we want to reconstruct is shown in figure 2

In all experiments the two transmitters operated simultaneously: transmitter 1 emitted a linear up-chirp $\sin(\omega_0[t + \alpha t^2])$, while transmitter 2 simultaneously emitted a linear down-chirp $\sin(\omega_0[t - \alpha t^2])$. Thus, there was an inherent ambiguity in the reflected waveforms as to the

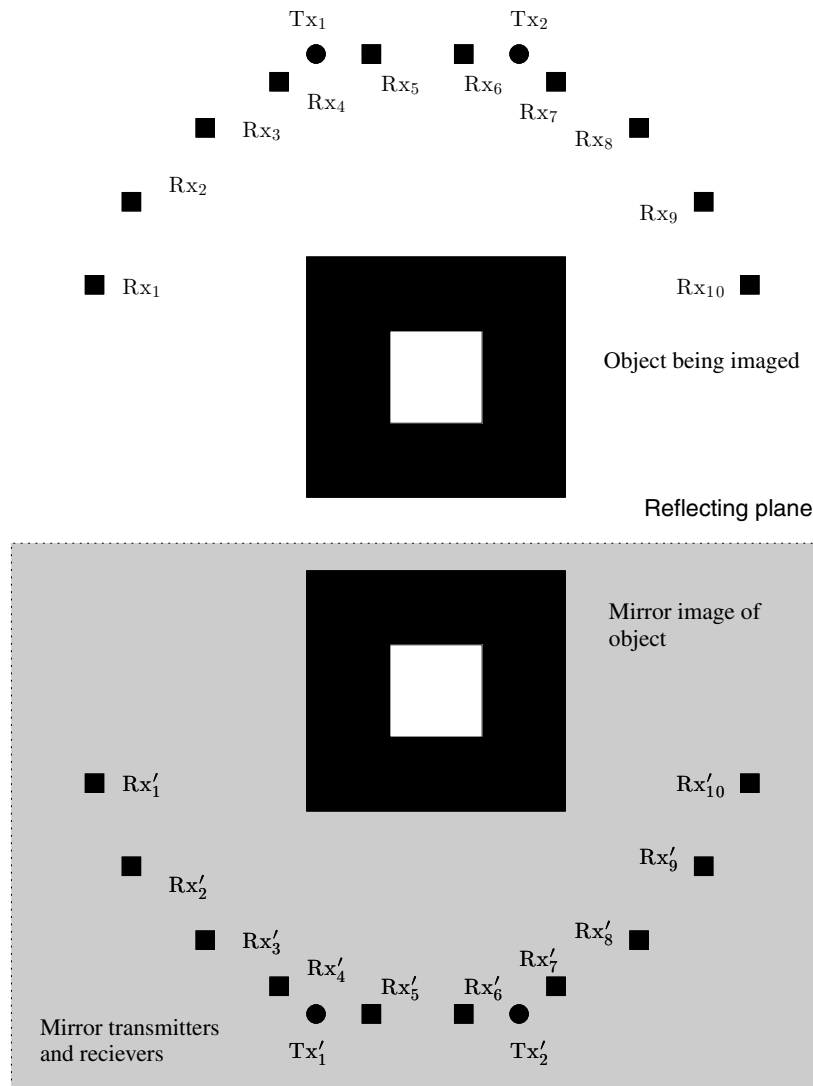


Figure 2. Distributed array with 2 transmitting elements (circles labeled Tx_1 and Tx_2), and 10 receiving elements (small squares labeled from Rx_1 to Rx_{10}). The elements are placed at equidistant points along an arc with radius 10λ , where λ is the wavelength corresponding to the center frequency of the transmitters. The target is indicated as a square with sides of 1.5λ , while the region of interest is $5\lambda \times 5\lambda$ around the target. The solid straight line indicates the location of a reflective mirror in our simple multi-path scenario. A gray box frames the mirror image of the object, as well as the mirror transmitters (labeled Tx'_1 and Tx'_2) and mirror receivers (labeled from Rx'_1 to Rx'_{10}).

origin of the energy. In our experiments we used $\omega_0 = 2\pi/\lambda$ and $\alpha = 0.1$, and generated waveforms of length 3 by subsequently applying a rectangular window, slightly tapered to adhere to the smoothness conditions. These waveforms were then sampled at a rate of $10/\lambda$.

In all of these results we used 250 terms in the SVD of \mathcal{H} . Additional terms did not affect the solution significantly for our noise-free simulations. However, in truncating the SVD we implicitly obtain a regularized solution.

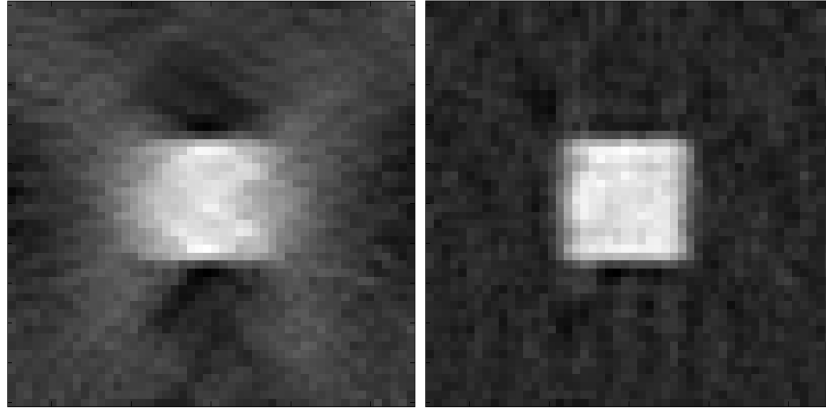


Figure 3. Images reconstructed using our method from theorem 1. In this case we used 2 transmitters and 10 receivers. For the free-space case (left) the reconstruction error was -5.7 dB. In the multi-path case (right) we get a reconstruction error of -11.2 dB.

We performed numerical experiments to demonstrate the performance of our image reconstruction method for the following cases: (1) free space, (2) multi-path environment, (3) reduced number of receivers, (4) measurements embedded in non-stationary noise.

5.3. Noise-free simulations

For the experiments (1)–(3) the measurements were free of noise, and the reflectivity function was deterministic. We therefore used the reconstruction formula in theorem 1. In this case we reconstruct a projection of the reflectivity function onto the range of \mathcal{H}^* . To measure how well the reconstruction approximates the true reflectivity function, we use the following relative L^2 norm to quantify the reconstruction error:

$$\text{Error} = 10 \log \left(\frac{\int |[\mathcal{H}^\dagger \mathcal{H}(V)](\mathbf{x}) - V(\mathbf{x})|^2 d\mathbf{x}}{\int |V(\mathbf{x})|^2 d\mathbf{x}} \right). \quad (63)$$

(1) *Free space.* In the left panel of figure 3, we see a reconstruction for the free-space scenario using our reconstruction method when we have 2 transmitters and 10 receivers distributed as indicated in figure 2. The reconstruction error as defined in (63) is here -5.7 dB.

(2) *Multi-path.* The right panel of figure 3 shows the reconstruction for our multi-path scenario when we have 2 transmitters and 10 receivers distributed as indicated in figure 2. The reconstruction error is in this case -11.2 dB.

We see that our method's use of the multi-path scattering improves the reconstruction. In particular we note that the vertical edges are much sharper when multi-path is present. In section 5.1 we showed that our multi-path scenario can be viewed as a free-space scenario with additional transmitters and receivers. Thus if we can exploit the multi-path returns properly, these additional antenna elements provide illumination of the object from new directions. This phenomenon is explained by the fact that only edges perpendicular to the bisector between the incident ray and the reflected ray are visible [28]. A similar effect was also observed in [22].

(3) *Reduced number of receivers.* To demonstrate the influence of the transmitter location and array sparsity, we remove five of the receiver elements and perform another free-space

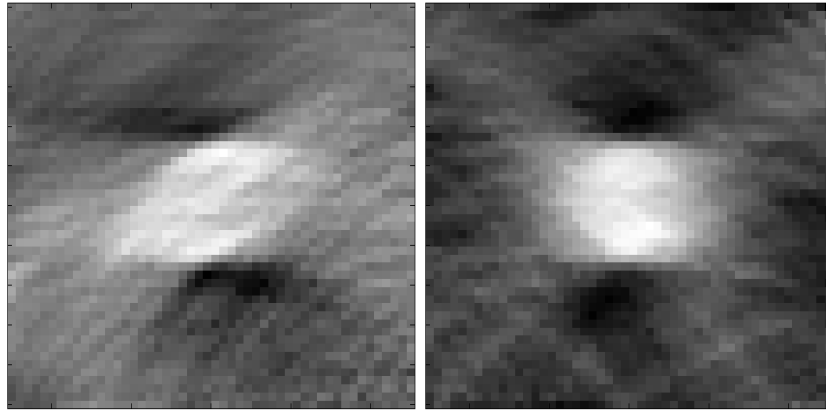


Figure 4. Free-space reconstruction with reduced number of receivers. Left: when only receiver elements 1–5 are active. Right: only receiver elements 1, 3, 5, 7 and 9 are active. Reconstruction errors for the left and the right images are -2.7 dB and -5.0 dB, respectively.

simulation. First we performed reconstruction with receivers 6–10 removed (receivers numbered from left to right in figure 2). Then we removed receivers 2, 4, 6, 8 and 10. Figure 4 shows reconstruction results from simulations with these reduced apertures. From figure 4 we see that reducing the aperture has led to artifacts in the reconstructed image. We observe the most significant image degradation when the aperture is reduced by removing elements 6–10. The explanation for this is given by the fact that the scattering measurements obtained for neighboring receivers contain similar information about the reflectivity function. Therefore, removing every second receiver does not result in significant information loss. However, since the information redundancy is less for receivers that are far apart, disabling elements 6–10 leaves us with significantly less information about the object that we want to reconstruct.

5.4. Statistical reconstruction

The results for simulation case (3) were obtained using the reconstruction formula in (45). The overall simulation setup is the same as for the deterministic case. However, here we add noise to our scattering measurements, and use a statistical model for the reflectivity function.

In our experiment we considered a wide-band $1/\omega$ -type noise model similar to that used in [26]. The noise was generated by filtering white noise in the frequency domain to obtain a power spectrum

$$S(\omega) = \frac{2\sigma^2}{1 + \omega^2}, \quad (64)$$

where $\sigma^2 = E[|n_i(t)|^2]$ is the noise variance for scattering measurements made at each receiver element. We considered a square object with unknown scattering strength c , i.e.,

$$V(\mathbf{x}) = c\chi(1.5\lambda\mathbf{x}). \quad (65)$$

Here χ is 1 on the unit square, and the scattering strength c is a Gaussian distributed random variable with zero mean and unit variance.

We define the *signal-to-noise ratio* (SNR) as follows:

$$\text{SNR} := \sup_t \sqrt{\frac{\text{E}[|\mathcal{H}(V)\mathbf{s}^k(t)|^2]}{\text{E}[|\mathbf{n}(t)|^2]}}, \quad (66)$$

where $\mathbf{n}(t)$ is the additive noise process. To evaluate the SNR, we estimated $\text{E}[|\mathcal{H}(V)\mathbf{s}^k(t)|^2]$ by averaging over 50 realizations of the reflectivity function, and found its peak value. We then scaled the additive noise variance to obtain the desired SNR.

In order to compute the operators \mathcal{M} , \mathcal{S} and \mathcal{E} (46)–(48), we used the eigenvalues and eigenfunctions U_p of $\mathcal{H}^*\mathcal{H}$ from our noise-free reconstructions. In particular, we did the following:

- We computed components (46) of the operator \mathcal{M} by numerically projecting our model for the reflectivity function (65) onto the eigenfunctions U_p and using $\text{E}[|c|^2] = 1$.
- To obtain \mathcal{E} , we first computed $\mathcal{U}_j\mathbf{s}_k(t)$ by performing noise-free scattering simulations from the reflectivity function U_j . To each vector element of this simulated scattering, we applied a filter with the impulse response $\frac{1}{1+\omega^2}$ (from (64) to obtain $\mathcal{R}_n\mathcal{U}_j\mathbf{s}_k(t)$. Finally, we computed the element $(\mathcal{E})_{ij}$ by taking the inner product between this filtered scattering simulation and an un-filtered scattering simulation from the reflectivity U_i , and summing over all our transmit vectors. For a particular SNR, we multiplied the whole operator by a constant corresponding to the scaling which was applied to the additive noise.

The quality of the reconstruction in the presence of additive noise is quantified by means of a relative mean-square error expressed in a decibel scale:

$$\text{MSE} := 10 \log \left(\frac{\int \text{E}[|\mathcal{H}^\dagger\mathcal{H}(V)](\mathbf{x}) - PV(\mathbf{x})|^2 d\mathbf{x}}{\int \text{E}[|V(\mathbf{x})|^2] d\mathbf{x}} \right). \quad (67)$$

This is clearly equivalent to using the MSE as defined in (42), and measures how well our statistical reconstruction approximates the deterministic one. Therefore, it measures the effect of the noise, and our ability to suppress this noise, rather than actual reconstruction performance relative to the actual object.

To compute PV in (67), we used the reconstructions from experiments (1) and (2), i.e., reconstructions without noise. The value for $\int \text{E}[|\mathcal{H}^\dagger\mathcal{H}(V)](\mathbf{x}) - PV(\mathbf{x})|^2 d\mathbf{x}$ was then estimated from 10 different reconstructions using different noise realizations. Finally, we computed $\int \text{E}[|V(\mathbf{x})|^2] d\mathbf{x}$ from (65) directly.

(4) *Simulations for statistical reconstruction.* Figure 5 shows examples of reconstruction in the presence of additive noise. The reconstruction is based on scattering from a unit square with unit scattering strength. The noise was added so that the measurements had an SNR of 20. In the top left panel of figure 5 we see a reconstruction for our free-space scenario, while in the top right panel we have a reconstruction for our multi-path scenario. In order to show the necessity of taking the additive noise into account, we have also included a deterministic free-space reconstruction in the lower left panel of figure 5. In the lower right panel of figure 5 we see the MSE as a function of SNR. Here, the solid line and dashed-dot line denote statistical reconstruction in the free-space case and the multi-path case, respectively. The MSE of the deterministic free-space reconstruction is shown as dotted line. The MSE was estimated according to equation (67) by averaging over 10 realizations of the scattering potential and the additive noise for each SNR. The MSE was then normalized relative to the free-space statistical reconstruction.

The MSE that we have plotted in figure 5 is measured relative to the noise-free reconstruction in each case. Thus, the MSE of the multi-path reconstruction is judged against a much better reference than the free-space reconstruction (see figure 3). As a result, the

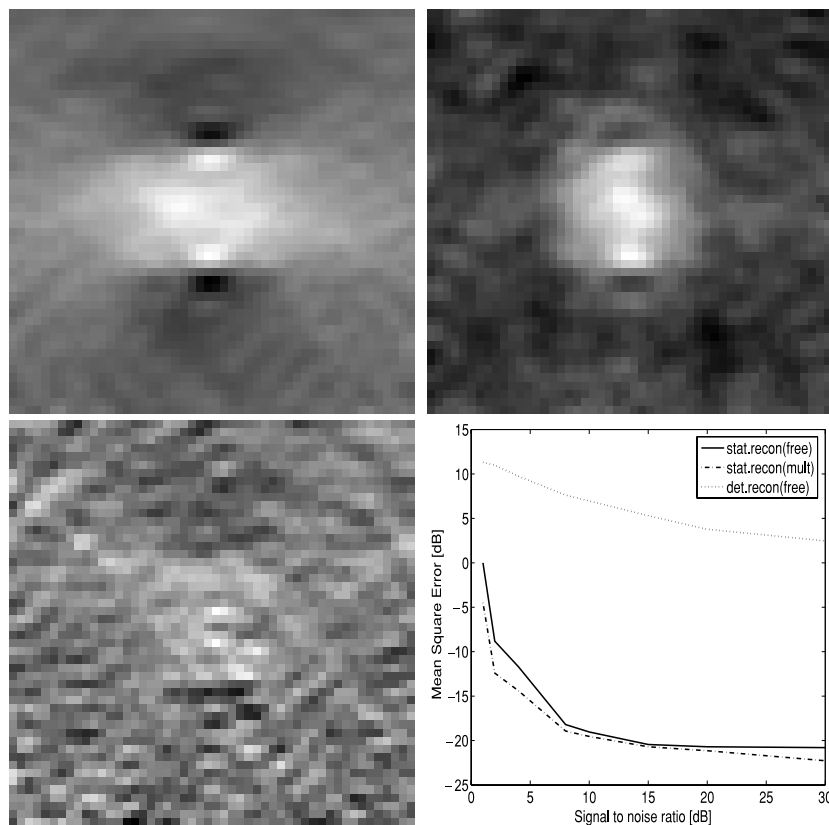


Figure 5. Reconstructed images in the presence of additive noise. Top left: statistical reconstruction in free-space with SNR = 20 dB. Top right: statistical reconstruction in multi-path with SNR = 20 dB. Bottom left: deterministic reconstruction in free space with SNR = 20 dB. Bottom right: MSE in the reconstructed images as a function of SNR.

MSE of the multi-path does not correctly portray the reconstruction improvement over the free-space reconstruction relative to the true object.

Comparing the deterministic and the statistic reconstruction, it is clear that additive noise corrupts the deterministic approach. Our deterministic reconstruction does not take noise information into account; it is not regularized beyond what is implicit in our inclusion of only the first 250 terms in the computation of the SVD. It is clear that a different number of terms in the SVD would result in images of different quality. However, it is beyond the scope of this paper to discuss regularization of the deterministic method.

6. Conclusion

In this paper we have derived an image reconstruction method for wide-band pulse-echo imaging using sparse distributed arrays operating in multi-path environments. The underlying mathematical model is based on a Green's function formulation of the scattering problem. Our model lends itself to a wide range of fields such as ultrasound, radar, sonar and seismic imaging, where wide-band transmit waveforms and distributed apertures are frequently used.

Our analysis is performed using a time-domain propagation model, and incorporates statistical information about the noise and the objects to be imaged. We derive an explicit time-domain reconstruction formula that minimizes the L^2 reconstruction error. This reconstruction formula lends itself to a rapid, parallel implementation.

An important concept in our work is the channel mapping, a mapping from the space of reflectivity functions to the corresponding scattering operator. This approach shows how to perform image reconstruction when multiple transmitters are activated simultaneously. In particular, we have presented a time-domain analysis by which we obtain explicit expressions for the singular value decomposition of the channel mapping in terms of scattering measurements and pre-computed basis functions. The pre-computed quantities that we use in the reconstruction take the form of scattering from a set of basis functions for the space of reflectivity functions.

Our work was presented in the regime of the distorted-wave Born approximation. Under this approximation, the channel mapping is linear. This allows us to use the machinery of Hilbert–Schmidt operators to find the inverse by means of the SVD. Although the concept of a channel mapping is valid without the Born approximation, the channel mapping would then no longer be linear, and a different formalism would be needed to obtain its inverse; this is beyond the scope of our current paper.

By reconstructing an image using a reduced set of basis functions, we are effectively compressing the image into a small number of coefficients. Our work therefore has interesting connections to compressive sensing. We leave an exploration of these connections for the future.

Acknowledgments

We are grateful to Air Force Office of Scientific Research⁴ (AFOSR) and the Defense Advanced Research Projects Agency (DARPA) for supporting this work under the agreements FA9550-04-1-0223, FA9550-07-1-0363, FA9550-06-1-0017 and FA8750-05-2-0285.

Appendix A. Wave propagation and scattering

For many imaging problems, an appropriate model for wave propagation is the scalar wave equation (1). For the background medium, fundamental solutions are defined by (2). The Green's function that we use is the outgoing fundamental solution; it is useful because it allows us to solve the wave equation with a source density $s(\mathbf{x}, t)$

$$\nabla^2 u^{\text{in}} - \frac{1}{c^2} \partial_t^2 u^{\text{in}} = s(\mathbf{x}, t)$$

by

$$u^{\text{in}}(\mathbf{x}, t) = \int g(\mathbf{x}, \mathbf{y}, t - \tau) s(\mathbf{y}, \tau) d\mathbf{y} d\tau. \quad (\text{A.1})$$

Here we use the source s to model an antenna or transducer; the corresponding field u^{in} is the wave radiated from the source (and which is incident on the scatterer V). For simplicity, we use an isotropic point-source model, namely $s(\mathbf{x}, t) = s(t)\delta(|\mathbf{x} - \mathbf{x}_0|)$. The analysis, however, holds also for the more general transmitter models.

⁴ Consequently, the US Government is authorized to reproduce and distribute reprints for governmental purposes notwithstanding any copyright notation thereon. The views and conclusions contained herein are those of the authors and should not be interpreted as necessarily representing the official policies or endorsements, either expressed or implied, of the Air Force Research Laboratory or the US Government.

Similarly, we use the Green's function to express the field u of (1) as a solution of the Lippmann–Schwinger equation:

$$u(\mathbf{x}, t) = u^{\text{in}}(\mathbf{x}, t) + \int g(\mathbf{x}, \mathbf{y}, t - \tau) V(\mathbf{y}) u(\mathbf{y}, \tau) \, d\mathbf{y}. \quad (\text{A.2})$$

We write $u(\mathbf{x}, t) = u^{\text{in}}(\mathbf{x}, t) + u^{\text{sc}}(\mathbf{x}, t)$ in (A.2):

$$u^{\text{sc}}(\mathbf{x}, t) = \int g(\mathbf{x}, \mathbf{y}, t - \tau) V(\mathbf{y}) \partial_{\tau}^2 u(\mathbf{y}, \tau) \, d\mathbf{y}. \quad (\text{A.3})$$

The solution u^{sc} depends nonlinearly on the perturbation V . We obtain a linear approximation by replacing the full field u in the integral by u^{in} :

$$u^{\text{sc}}(\mathbf{x}, t) = \int g(\mathbf{x}, \mathbf{y}, t - \tau) V(\mathbf{y}) \partial_{\tau}^2 u^{\text{in}}(\mathbf{y}, \tau) \, d\mathbf{y}. \quad (\text{A.4})$$

This is often referred to as the *distorted-wave Born approximation*; it is a reasonable approximation as long as the perturbation V is small. By using (A.1) to express u^{in} , we can write (A.4) as a bilinear mapping from reflectivity function V and transmit waveform $s(t)$ to the field at position \mathbf{x}

$$u^{\text{sc}}(\mathbf{x}, t) = \int g(\mathbf{x}, \mathbf{y}, t - \tau') \partial_{\tau'}^2 g(\mathbf{y}, \mathbf{x}_0, \tau' - \tau) \quad (\text{A.5})$$

$$\times V(\mathbf{y}) s(\tau) \, d\tau \, d\tau' \, d\mathbf{y}. \quad (\text{A.6})$$

Finally, we use superposition to express the scattered field resulting from an aperture with m transmitters located at positions \mathbf{x}^j transmitting waveforms s_j as

$$u^{\text{sc}}(\mathbf{x}, t) = \sum_{j=1}^m \int g(\mathbf{x}, \mathbf{y}, t - \tau') \partial_{\tau'}^2 g(\mathbf{y}, \mathbf{x}^j, \tau' - \tau) V(\mathbf{y}) s_j(\tau) \, d\tau \, d\tau' \, d\mathbf{y}. \quad (\text{A.7})$$

Appendix B. Proof of lemma 1

In order to show this result, $\mathcal{H}(V)$ will be factored into a composition of two bounded linear operators—one of which will be HS. The desired result follows from the fact that composition of a bounded linear operator with an HS operator is HS [29, theorem 6.10].

In order to keep the notation simple, we will give a proof for the scalar case ($m = n = 1$), and thus avoid adding notation for each matrix element of the operator $\mathcal{H}(V)$. The same proof holds for each matrix element separately also for the general case. Therefore, since a finite linear combination of HS operators is HS, the result holds also for finite m and n .

By assumption 2, the transmit waveforms are in the Sobolev space $\overset{\circ}{\text{H}}^{(5+\rho)/2}(0, T_0)$.

Let ∂_t^k denote the differentiation operator of order k . (When k is not an integer, this operator is a pseudodifferential operator.) The operators ∂_t^k are linear bounded operators

$$\partial_t^k : \text{H}^K(\mathbb{R}) \rightarrow \text{L}^2(\mathbb{R}), \quad \text{for } k \leq K. \quad (\text{B.1})$$

Let $\rho > 0$ be a fixed constant. We use the Fourier transform to write $\mathcal{H}(V)$ from (7) as follows:

$$\mathcal{H}(V)s(t) = \int e^{i\omega t} \frac{\hat{g}(z^1, \mathbf{y}, \omega) \hat{g}(\mathbf{y}, \mathbf{x}^1, \omega) V(\mathbf{y})}{2\pi} \, d\mathbf{y} (-\omega^2) \hat{s}(\omega) \, d\omega \quad (\text{B.2})$$

$$= \int e^{i\omega t} \frac{\hat{g}(z^1, \mathbf{y}, \omega) \hat{g}(\mathbf{y}, \mathbf{x}^1, \omega) V(\mathbf{y})}{2\pi [1 + (i\omega)^{\frac{1}{2} + \rho}]} \, d\mathbf{y} [1 + (i\omega)^{\frac{1}{2} + \rho}] (-\omega^2) \hat{s}(\omega) \, d\omega. \quad (\text{B.3})$$

We use this to factor $\mathcal{H}(V)$ into a composition of two linear operators

$$\mathcal{H}(V) = \mathcal{A}(V)(\partial_t^2 + \partial_t^{\frac{5}{2}+\rho}). \tag{B.4}$$

where $\mathcal{A}(V)$ is

$$\mathcal{A}(V)s(t) = \int e^{i\omega t} \frac{\hat{g}(z^1, \mathbf{y}, \omega)\hat{g}(\mathbf{y}, \mathbf{x}^1, \omega)V(\mathbf{y})}{2\pi[1 + (i\omega)^{\frac{1}{2}+\rho}]} d\mathbf{y} s(\omega) d\omega \tag{B.5}$$

$$= \int A_V(t - \tau)s(\tau) d\tau. \tag{B.6}$$

As noted above, $g(\partial_t^2 + \partial_t^{\frac{5}{2}+\rho})$ is a bounded operator from $H^{\frac{5}{2}+\rho}(\mathbb{R})$ to $L^2(\mathbb{R})$. We show below that $\mathcal{A}(V)$ is a HS operator on $L^2(\mathbb{R})$. Therefore, if we consider $\mathcal{H}(V)$ as an operator from $H^{\frac{5}{2}+\rho}(\mathbb{R})$ to $L^2(\mathbb{R})$, then we have obtained a factorization of $\mathcal{H}(V)$ into two bounded linear operators. This shows that the composite operator $\mathcal{H}(V)$ is HS from $H^{\frac{5}{2}+\rho}(0, T_0)$ to $L^2(\mathbb{R})$.

It remains to show that $\mathcal{A}(V)$ is a HS operator on $L^2(\mathbb{R})$. First we note that the convolution kernel $A_V(t)$ is in $L^2(\mathbb{R})$ since

$$\|A_V\|_2^2 = \int \left| \int \frac{\hat{g}(z^1, \mathbf{y}, \omega)\hat{g}(\mathbf{y}, \mathbf{x}^1, \omega)V(\mathbf{y})}{(2\pi)^2[1 + (i\omega)^{\frac{1}{2}+\rho}]^2} d\mathbf{y} \right|^2 d\omega \tag{B.7}$$

$$\leq C^2 \left(\int_{\Omega} |V(\mathbf{y})|^2 d\mathbf{y} \right) \int \frac{1}{1 + |\omega|^{1+2\rho}} d\omega < \infty, \tag{B.8}$$

where we have used the bounds for the Green's function from assumption 1. Let now $\chi_{(0, T_0)}$ be the characteristic function for the interval $(0, T_0)$. We will consider waveforms s which are supported on the interval $(0, T_0)$. For such waveforms we will trivially modify the operator $\mathcal{A}(V)$ as follows:

$$\mathcal{A}(V)s = \int A_V(t - \tau)\chi_{(0, T_0)}(\tau)s(\tau) d\tau. \tag{B.9}$$

Since $A_V(t) \in L^2(\mathbb{R})$, the modified integral kernel $A_V(t - \tau)\chi_{(0, T_0)}(\tau) \in L^2(\mathbb{R} \times (0, T_0))$. Hence, the operator $\mathcal{A}(V)$ is HS [29, Theorem 6.11].

Appendix C. Proof of lemma 2

Proof of part (1). First we show that \mathcal{G}_y is bounded for each \mathbf{y} . This follows from the assumptions about the Green's function. Let e be a unit vector in the space of transmit vectors. Then, writing the norm of a vector as $\|v\| = v^H \cdot v$, we have

$$\|\mathcal{G}_y e\|^2 = \int \left(\int G(\mathbf{y}, t - \tau')e(\tau') d\tau' \right)^H \cdot \int G(\mathbf{y}, t - \tau)e(\tau) d\tau dt \tag{C.1}$$

$$= \int (\hat{G}(\mathbf{y}, \omega)\hat{e}(\omega))^H \cdot \hat{G}(\mathbf{y}, \omega)\hat{e}(\omega) d\omega \tag{C.2}$$

$$= \int \sum_{ij} \hat{e}_j(\omega)\overline{\hat{G}_{ij}(\mathbf{y}, \omega)}\hat{G}_{ij}(\mathbf{y}, \omega)\hat{e}_j(\omega) d\omega \tag{C.3}$$

$$= \int \sum_{ij} |\hat{G}_{ij}(\mathbf{y}, \omega)|^2 |\hat{e}_j(\omega)|^2 d\omega \tag{C.4}$$

$$\leq C^2 \int (1 + |\omega|^{5+\rho}) |\hat{\rho}_j(\omega)|^2 d\omega = C^2 \|e\|^2. \quad (\text{C.5})$$

Here C is the constant in assumption 1 and $\rho > 0$. Going from (C.1) to (C.2) we have employed Parseval's identity to write inner-product in the temporal frequency domain. (C.4) is obtained from (C.3) by the Cauchy–Schwarz inequality. Then (C.5) follows from writing out G_{ij} in terms of the Green's function according to (6), and applying assumption 1 in concert with (16).

Proof of part (2). This follows from the fact that the bound in part (1) is uniform.

Proof of part (3). Let now $\{e^k\}$ be an orthonormal basis for the space of transmit waveforms. The inner product between $\mathcal{H}(V)$ and \mathcal{A} is

$$\langle \mathcal{H}(V), \mathcal{A} \rangle_{\text{HS}} = \sum_k \langle \mathcal{A}^* \mathcal{H}(V) e^k, e^k \rangle_S, \quad (\text{C.6})$$

where $\langle \cdot, \cdot \rangle_S$ is defined in (16). The action of $\mathcal{A}^* \mathcal{H}(V)$ on $e^k(t)$ is further computed from (7) as

$$\mathcal{A}^* \mathcal{H}(V) e^k(t) = \mathcal{A}^* \int G(\mathbf{y}, t, \tau) e^k(\tau) d\tau V(\mathbf{y}) d\mathbf{y}. \quad (\text{C.7})$$

Inserting (C.7) into (C.6) and bringing the inner product inside the integral, we obtain

$$\langle \mathcal{H}(V), \mathcal{A} \rangle_{\text{HS}} = \int V(\mathbf{y}) \sum_k \langle \mathcal{A}^* \mathcal{G}_y e^k, e^k \rangle_S d\mathbf{y}. \quad (\text{C.8})$$

Note that since \mathcal{A} is also HS, the adjoint \mathcal{A}^* is HS. Since \mathcal{G}_y is bounded, $\mathcal{A}^* \mathcal{G}_y$ is also HS. We therefore use (13) to write the sum over k in (C.8) in terms of a trace:

$$\langle \mathcal{H}(V), \mathcal{A} \rangle_{\text{HS}} = \int V(\mathbf{y}) \text{Tr}\{\mathcal{A}^* \mathcal{G}_y\} d\mathbf{y} \quad (\text{C.9})$$

$$= \langle V, \overline{\text{Tr}\{\mathcal{G}_y \mathcal{A}^*\}} \rangle. \quad (\text{C.10})$$

From this follows that the adjoint of \mathcal{H} applied to \mathcal{A} is

$$\mathcal{H}^* \mathcal{A} = \overline{\text{Tr}\{\mathcal{G}_y \mathcal{A}^*\}} \quad (\text{C.11})$$

for almost every \mathbf{y} .

Appendix D. Proof of theorem 2

Our first task is to obtain a simplified expression for the MSE (42). To do this, we need the following ingredients:

- (i) We write the action of the operator \mathcal{B} in terms of the $\{U_p\}$:

$$\mathcal{B}(f)(\mathbf{x}) = \sum_p \sum_{p'} b_{pp'} \langle f, U_{p'} \rangle U_p(\mathbf{x}) = \sum_p \sum_{p'} b_{pp'} \int f(\mathbf{y}) \overline{U_{p'}(\mathbf{y})} d\mathbf{y} U_p(\mathbf{x}). \quad (\text{D.1})$$

- (ii) From the spectral decomposition (28) and definition (29), we obtain a spectral decomposition for \mathcal{H} :

$$\mathcal{H}(V) = \sum_p \langle V, U_p \rangle \sqrt{\lambda_p} \mathcal{U}_p. \quad (\text{D.2})$$

(iii) We split $\mathcal{H}^*\mathcal{H}(V)$ into the term corresponding to V and to noise, using first (32) and (37):

$$\begin{aligned} \mathcal{H}^*\mathcal{H}(V) &= \sum_k (\langle \mathcal{H}(V)s^i, \mathcal{G}_x s^k \rangle + \langle \mathbf{n}, \mathcal{G}_x s^k \rangle) \\ &= \underbrace{\sum_k \sum_p \langle V, U_p \rangle \sqrt{\lambda_p} \langle \mathcal{U}_p s^k, \mathcal{G}_x s^k \rangle}_{A_V(\mathbf{x})} + \underbrace{\sum_k \langle \mathbf{n}, \mathcal{G}_x s^k \rangle}_{A_n(\mathbf{x})}, \end{aligned}$$

where we have used (D.2) in the second line.

Using (D.1) with $f = \mathcal{H}^*\mathcal{H}(V) = A_V(\mathbf{x}) + A_n(\mathbf{x})$ and $V^{\mathcal{B}} = \mathcal{B}[\mathcal{H}^*\mathcal{H}(V)]$, we have a finite-sum approximation to (42):

$$\begin{aligned} \text{MSE}^N(\mathcal{B}) &:= \int \mathbb{E} \left[\left| \sum_{p,p'}^N b_{p,p'} \langle A_V + A_n, U_{p'} \rangle \right|^2 \right] d\mathbf{x} \\ &= \sum_p \mathbb{E} \left[\left| \sum_{p'} b_{p,p'} \langle A_V + A_n, U_{p'} \rangle - \langle V, U_p \rangle \right|^2 \right], \end{aligned} \tag{D.3}$$

where we have used the orthonormality of the U_p to write $\| \sum c_p U_p \|^2 = \sum |c_p|^2$. In (D.3), we recall that the dependence on noise appears only in A_n , and use the assumptions that the noise has zero mean, and is uncorrelated with the reflectivity function V and with noise from other measurements to throw away cross-terms in (D.3) and arrive at

$$\text{MSE}^N(\mathcal{B}) := \sum_p \mathbb{E} \left[\left| \sum_{p'} b_{p,p'} \langle A_V, U_{p'} \rangle - \langle V, U_p \rangle \right|^2 \right] + \sum_p \mathbb{E} \left[\left| \sum_{p'} b_{p,p'} \langle A_n, U_{p'} \rangle \right|^2 \right]. \tag{D.4}$$

The term $\langle A_V, U_{p'} \rangle$ we write as

$$\begin{aligned} \langle A_V, U_{p'} \rangle &= \left\langle \sum_k \sum_p \langle V, U_p \rangle \sqrt{\lambda_p} \langle \mathcal{U}_p s^k, \mathcal{G}_x s^k \rangle, U_{p'} \right\rangle \\ &= \sum_k \sum_p \langle V, U_p \rangle \sqrt{\lambda_p} \langle \mathcal{U}_p s^k, \sqrt{\lambda_{p'}} \mathcal{U}_{p'} s^k \rangle \\ &= \lambda_{p'} \langle V, U_{p'} \rangle, \end{aligned} \tag{D.5}$$

where we have used the fact that

$$\sum_k \langle \mathcal{U}_p s^k, \mathcal{U}_{p'} s^k \rangle = \langle \mathcal{U}_p, \mathcal{U}_{p'} \rangle_{\text{HS}} = \frac{1}{\sqrt{\lambda_p \lambda_{p'}}} \langle \mathcal{H}^*\mathcal{H}(U_p), U_{p'} \rangle = \frac{\lambda_p}{\sqrt{\lambda_p \lambda_{p'}}} \langle U_p, U_{p'} \rangle = \delta_{p,p'}. \tag{D.6}$$

With (D.5), (D.4) becomes

$$\text{MSE}^N(\mathcal{B}) := \sum_p \mathbb{E} \left[\left| \sum_{p'} b_{p,p'} \lambda_{p'} \langle V, U_{p'} \rangle - \langle V, U_p \rangle \right|^2 \right] + \sum_p \mathbb{E} \left[\left| \sum_{p'} b_{p,p'} \langle A_n, U_{p'} \rangle \right|^2 \right]. \tag{D.7}$$

Since $\text{MSE}^N(\mathcal{B})$ increases monotonely as N goes to infinity, we can interchange the order of expectation and the limit as $N \rightarrow \infty$ to obtain

$$\text{MSE}(\mathcal{B}) = \sum_p \mathbb{E} \left[\left| \sum_{p'} b_{pp'} \lambda_{p'} \langle V, U_{p'} \rangle - \langle V, U_p \rangle \right|^2 \right] \quad (\text{D.8})$$

$$+ \sum_{pp'q'} b_{pp'} \overline{b_{pq'}} \sqrt{\lambda_{p'}} \sqrt{\lambda_{q'}} \mathbb{E}[\langle \mathbf{n}^k, \mathcal{U}_{p'} \mathbf{s}^k \rangle \overline{\langle \mathbf{n}^k, \mathcal{U}_{q'} \mathbf{s}^k \rangle}]. \quad (\text{D.9})$$

We can evaluate $\sum_k \mathbb{E}[\langle \mathbf{n}^k, \mathcal{U}_{p'} \mathbf{s}^k \rangle \overline{\langle \mathbf{n}^k, \mathcal{U}_{q'} \mathbf{s}^k \rangle}]$ from (D.9) as follows:

$$\sum_k \mathbb{E}[\langle \mathbf{n}, \mathcal{U}_{p'} \mathbf{s}^k \rangle \overline{\langle \mathbf{n}, \mathcal{U}_{q'} \mathbf{s}^k \rangle}] = \sum_{kij} \int \overline{(\mathcal{U}_{p'} \mathbf{s}^k)_i(t_1)} \mathbb{E}[n_i(t_1) \overline{n_j(t_2)}] (\mathcal{U}_{q'} \mathbf{s}^k)_j(t_2) dt_1 dt_2 \quad (\text{D.10})$$

$$= \sum_{kij} \int \overline{(\mathcal{U}_{p'} \mathbf{s}^k)_i(t_1)} R_i(t_1, t_2) \delta_{ij} (\mathcal{U}_{q'} \mathbf{s}^k)_j(t_2) dt_1 dt_2 \quad (\text{D.11})$$

$$= \sum_k \langle \mathcal{R}_n \mathcal{U}_{q'} \mathbf{s}^k, \mathcal{U}_{p'} \mathbf{s}^k \rangle \quad (\text{D.12})$$

$$= \text{Tr}\{\mathcal{U}_{p'}^* \mathcal{R}_n \mathcal{U}_{q'}\}. \quad (\text{D.13})$$

Here \mathcal{R}_n is an integral operator whose kernel is a diagonal matrix with functions $R_i(t_1, t_2)$ from (39) along the diagonal. The operator \mathcal{R}_n is a bounded operator on L^2 under both assumptions (6.2a) and (6.2b). In the case of assumption (6.2b) we may apply Young's theorem to show this fact [30]. Since \mathcal{U}_p is HS, it then follows that $\text{Tr}\{\mathcal{U}_{q'}^* \mathcal{R}_n \mathcal{U}_{q'}\}$ is finite.

If we insert (40) and (D.13) into (D.9) we obtain

$$\text{MSE}(\mathcal{B}) = \sum_p \mathbb{E} \left[\left| \sum_{p'} (b_{pp'} \lambda_{p'} - \delta_{pp'}) \sum_r c_r \langle V_r, U_{p'} \rangle \right|^2 \right] \quad (\text{D.14})$$

$$+ \sum_{pp'q'} \overline{b_{pq'}} \sqrt{\lambda_{q'}} \text{Tr}\{\mathcal{U}_{p'}^* \mathcal{R}_n \mathcal{U}_{q'}\} b_{pp'} \sqrt{\lambda_{p'}}. \quad (\text{D.15})$$

The random variables c_i in the KL expansion are statistically independent, i.e., $\mathbb{E}[c_i \overline{c_j}] = 0$ for $i \neq j$. Therefore,

$$\text{MSE}(\mathcal{B}) = \sum_{pp'q'} (\overline{b_{pq'} \lambda_{q'}} - \delta_{pq'}) \quad (\text{D.16})$$

$$\times \sum_r \mathbb{E}[|c_r|^2] \langle V_r, U_{p'} \rangle \overline{\langle V_r, U_{q'} \rangle} (b_{pp'} \lambda_{p'} - \delta_{pp'}) \quad (\text{D.17})$$

$$+ \sum_{pp'q'} \overline{b_{pq'}} \sqrt{\lambda_{q'}} \text{Tr}\{\mathcal{U}_{p'}^* \mathcal{R}_n \mathcal{U}_{q'}\} b_{pp'} \sqrt{\lambda_{p'}}.$$

We now define the operators \mathcal{M}, \mathcal{S} and \mathcal{E} by their coefficients in the $\{U_p\}$ basis via (46)–(48). Using these operators, we can re-write (D.16) as

$$\text{MSE}(\mathcal{B}) = \text{Tr}\{(\mathcal{B}\mathcal{S} - I)\mathcal{M}(\mathcal{B}\mathcal{S} - I)^* + \mathcal{B}\mathcal{S}^{\frac{1}{2}}\mathcal{E}\mathcal{S}^{\frac{1}{2}}\mathcal{B}^*\}. \quad (\text{D.18})$$

The variational derivative of $\text{MSE}(\mathcal{B})$ with respect to \mathcal{B} is

$$\text{MSE}(\mathcal{B} + \delta\mathcal{B}) - \text{MSE}(\mathcal{B}) = \text{Tr}\{2 \text{Re}[(\mathcal{B}\mathcal{S} - I)\mathcal{M}\delta\mathcal{B}^* + \mathcal{B}\mathcal{S}^{\frac{1}{2}}\mathcal{E}\mathcal{S}^{\frac{1}{2}}\delta\mathcal{B}^*]\} + o(\|\delta\mathcal{B}\|^2). \quad (\text{D.19})$$

Since MSE is a quadratic functional of \mathcal{B} , the global minimum is characterized by

$$\text{Tr}\{2 \text{Re}[(\mathcal{B}\mathcal{S} - \mathcal{I})\mathcal{M}\mathcal{S} + \mathcal{B}\mathcal{S}^{\frac{1}{2}}\mathcal{E}\mathcal{S}^{\frac{1}{2}}]\delta\mathcal{B}^*\} = 0 \quad (\text{D.20})$$

for all perturbations $\delta\mathcal{B}^*$. This leads to the following MMSE solution for \mathcal{B}

$$\mathcal{B} = \mathcal{M}\mathcal{S}(\mathcal{S}\mathcal{M}\mathcal{S} + \mathcal{S}^{\frac{1}{2}}\mathcal{E}\mathcal{S}^{\frac{1}{2}})^{\dagger} \quad (\text{D.21})$$

and the resulting reconstruction formula of theorem 2 as stated in (45) follows.

References

- [1] Natterer F and Wubbeling F 2001 *Mathematical Methods in Image Reconstruction* (Philadelphia: SIAM)
- [2] Bishop T N, Bube K P, Cutler R T, Langan R T, Loève P L, Resnick J R, Shuey R T, Spindler D A and Wyld H W 1985 Tomographic determination of velocity and depth in laterally varying media *Geophysics* **50** 903–23
- [3] Glover G H and Sharp J L 1977 Reconstruction of ultrasound propagation speed distribution in soft tissue *IEEE Trans. Sonics Ultrason.* **24** 229–34
- [4] Lu C, Lin J, Chew W and Otto G 1996 Image reconstruction with acoustic measurements using distorted Born iteration method *Ultrason. Imaging* **18** 140–56
- [5] Waag R C, Lin F, Varslot T and Astheimer J P 2007 An eigenfunction method for the reconstruction of large-scale and high-contrast objects *IEEE Trans. Sonics Ultrason.* **54** 1316–32
- [6] Johnson S A, Borup D T, Wiskin J W, Natterer F, Wuebling F, Zhang Y and Olsen S C 1999 Apparatus and method for imaging with wavefields using inverse scattering techniques, US Patent 6,005,916
- [7] Bond E, Hagness S and Veen B 2003 Microwave imaging via space-time beamforming for early detection of breast cancer *IEEE Trans. Antennas Propag.* **51** 1690–705
- [8] Guo B, Wang Y, Li J, Stoica P and Wu R 2006 Microwave imaging via adaptive beamforming methods for breast cancer detection *J. Electromagn. Waves Appl.* **20** 53–63
- [9] Cheney M 2001 A mathematical tutorial on synthetic aperture radar *SIAM Rev.* **43** 301–12
- [10] Holm S, Elgetun H and Dahl G 1997 Properties of the beampattern of weight- and layout-optimized sparse arrays *IEEE Trans. Ultrason. Ferroelectr. Freq. Control* **44** 983–91
- [11] Trucco A and Murino V 1999 Stochastic optimization of linear sparse arrays *IEEE J. Ocean Eng.* **24** 291–9
- [12] Swift M, Riley J, Lourey S and Booth L 1999 An overview of the multistatic sonar program in Australia *Proc. Int. Symp. on Signal Processing and its Applications (Queensland, Australia)* pp 321–4
- [13] Eickstedt D and Schmidt H 2003 A low-frequency sonar for sensor-adaptive, multistatic, detection and classification of underwater targets with AUVs *Proc. Oceans* pp 1440–7
- [14] Adve R, Schneible R, Genello G and Antonik P 2005 Waveform-space-time adaptive processing for distributed aperture radars *Proc. 2005 IEEE Radar Conf. (Arlington, VA, USA)* pp 93–7
- [15] Adve R, Schneible R and McMillan R 2003 Adaptive space/frequency processing for distributed apertures *Proc. 2003 IEEE Radar Conf. (Huntsville, AL, USA)* pp 160–4
- [16] Adve R 2003 Sub-optimal adaptive processing for distributed aperture radars *Proc. 2nd Waveform Diversity Workshop, Verona, NY* pp 160–4
- [17] Fishler E, Haimovich A, Blum R, Cimini L, Chizhik D and Valenzuela R 2006 Spatial diversity in radars—models and detection performance *IEEE Trans. Signal Process.* **54** 823–838
- [18] Bekkerman I and Tabrikian J 2006 Target detection and localization using MIMO radars and sonars *IEEE Trans. Signal Process.* **54** 3873–83
- [19] Fletcher A and Robey F 2003 Performance bounds for adaptive coherence of sparse array radar *Proc. 11th Conf. Adaptive Sensors Array Processing, Lexington (MA)*
- [20] Rabideau D 2003 Ubiquitous MIMO digital array radar *Proc. 37th Asilomar Conf. Signals, Systems, Computers (Pacific Grove, CA, USA)* pp 1057–64
- [21] Dennison M and Devaney A 2004 Inverse scattering in inhomogeneous background media: II. multi-frequency case and SVD formulation *Inverse Problems* **20** 1307–24
- [22] Devaney A and Dennison M 2003 Inverse scattering in inhomogeneous background media *Inverse Problems* **19** 855–70
- [23] Yazıcı B and Xie G 2006 Wideband extended range—doppler imaging and waveform design in the presence of clutter and noise *IEEE Trans. Inf. Theory* **52** 4563–80
- [24] Engl H, Hanke M and Neubauer A 2000 *Regularization of Inverse Problems* (The Netherlands: Kluwer)
- [25] Todorovic P 1992 *An Introduction to Stochastic Processes and their Applications (Statistics)* (New York: Springer)

- [26] Yazıcı B, Cheney M and Yarman C E 2006 Synthetic aperture inversion for an arbitrary flight trajectory in the presence of noise and clutter *Inverse Problems* **22** 1705–29
- [27] Nolan C J, Cheney M, Dowling T and Gaburro R 2006 Enhanced angular resolution from multiply scattered waves *Inverse Problems* **22** 1817–34
- [28] Yarman C E, Yazıcı B and Cheney M 2008 Bistatic synthetic aperture radar imaging for arbitrary flight trajectories *IEEE Trans. Image Process.* **17**(1) 84–93
- [29] Weidmann J 1980 *Linear Operators in Hilbert Spaces* (New York: Springer)
- [30] Adams R and Fournier J 2003 *Sobolev Spaces* 2nd edn (The Netherlands: Elsevier)